Fabrication and Characterization of Single-Crystal Metal-Assisted Chemically Etched Rough Si Nanowires for Lithium-ion Battery Anodes

W. McSweeney[1], O. Lotty[2,3], J. D. Holmes[2,3], and C. O'Dwyer[1,4]

[1] *Department of Physics and Energy, and Materials and Surface Science Institute, University of Limerick, Limerick, Ireland*
[2] *Materials and Supercritical Fluids Group, Department of Chemistry and the Tyndall National Institute, University College Cork, Cork, Ireland*
[3] *Centre for Research on Adaptive Nanostructures and Nanodevices (CRANN), Trinity College Dublin, Dublin 2, Ireland*
[4] *Charles Parsons Initiative on Energy and Sustainable Environment, University of Limerick, Limerick, Ireland*

Silicon nanowires were fabricated by a metal assisted chemical (MAC) etching process and routes toward ohmic contacting of substrates for Li-ion battery anode application were developed. Si nanowire layers are comprised of wires that are single crystal with rough outer surfaces. The nanowires are epitaxial with the underlying Si(100) substrate, maintain equivalent doping density and crystal orientation, and are coated with a stoichiometric SiO_2. Electrical backside contacting using an In-Ga eutectic allows low-resistance ohmic contacts to low-doped nanowire electrodes for electrochemical testing.

Introduction

The preparation of large-area uniform nanostructure arrays, especially through controllable, simple approaches is an important aspect for the application of nanoscale materials in energy storage and conversion devices such as solar cells and lithium-ion batteries. Improving specific capacities and energy densities can also benefit from controlled, high surface area materials. Si has been shown to have a theoretical specific capacity of ~4,200 mAh g^{-1} (1,2) during operation as a lithium battery anode therefore and has attracted tremendous research interest because of its high capacity and significant cycle life improvement through the use of nanoscale Si (3). The advantage of Si nanowires (NWs) over the bulk Si material is that low-dimensional NWs can accommodate the ~400% volume change upon lithium insertion and removal in Si (4,5). Considerable progress has been made concerning nano-structured Si as an active (insertion) and passive (scaffold) anode material (6-9) and the viability of the approach looks promising. While large-scale tests in batteries are not yet available, all results obtained so far indicate that nano-structured Si might meet the majority of battery requirements; the ubiquitous supply of high quality bulk and nanoscale Si and the need for greener, recyclable batteries will promote its development. Recent approaches focused on the quality and development of ordered nanoscale wire and porous arrays in Si for this purpose (10,11).

Metal-assisted chemical (MAC) etching is a process where Si NWs can be fabricated by etching a Si wafer with the aid of metal catalyst particles (12). This is generally achieved with a composition of silver ions and an aqueous solution of

hydrofluoric acid (HF). According to a reduction–oxidation reaction proposed by Li *et al.* (13), hole injection is provided by the reduction of the solution at the catalyst metal (in this instance Ag). Since injected holes diffuse rapidly away from Ag particles, etching is confined to areas near the Ag. This behaviour makes MAC etching a simple and effective method for preparing arrays of Si nanowires. The advantage of MAC etched NWs over NWs formed by different methods *e.g.* vapor-liquid-solid (VLS) is that the relieved NWs are etched features of the starting substrate and are thus directly contacted to the substrate current collector. Additionally, the NW crystal orientation and doping density mimics the underlying substrate (in this instance in a (100) direction), while VLS NWs preferentially grow in the [111] and [112] directions which can vary with wire dimension and synthetic growth conditions (4,6).

Here, we detail the formation and characterization of Si NWs by MAC etching from a bulk Si wafer for use as lithium-ion battery anodes. The NW morphology and crystal structure were characterized by scanning electron microscopy (SEM) and detailed transmission electron microscopy (TEM) and convergent beam electron diffraction (CBED) methods, which show that the NWs have a rough outer surface but are entirely phase pure. X-ray diffraction (XRD), energy dispersive X-ray spectroscopy (EDX) and X-ray photoelectron spectroscopy (XPS) investigations confirm that all NWs retain their bulk (100) orientation and their surfaces are coated with stoichiometric SiO_2 of 1-2 nm thickness. Investigations of electrical contacting methods show that high resistivity, low doped p-type wafers can be ohmically contacted using In-Ga eutectic on a copper current collector.

Experimental

The NWs are fabricated by metal-assisted chemical (MAC) etching of a bulk single crystal Si wafer. To form SiNW layers, 200 mm diameter lightly p-doped Si (100) wafers (680 μm thickness) with a native oxide layer (~2-5 nm thick) were used. Each wafer was cut to a size of 5 mm × 10 mm and then cleaned using iso-propyl-alcohol (IPA) before etching. Wafer coupons were sonicated for two cycles in IPA for 20 mins at 40 ^{o}C and dried under nitrogen. Some substrates had polyimide tape protecting the unpolished side during etching reactions. Substrates were immersed for two hours in a heated solution of 10% HF containing 0.04 M $AgNO_3$ and maintained at 50 °C using a thermostated water bath. The oxidation and dissolution of Si consumes holes in the cathode and the Ag^+ reduces, which creates a standard reduction potential causing etching at the nanowire surface surrounding the Ag just as an electrical bias induces etching of a Si wafer surface in an aqueous solution containing only HF in the absence of Ag^+, summarized in Fig. 1.

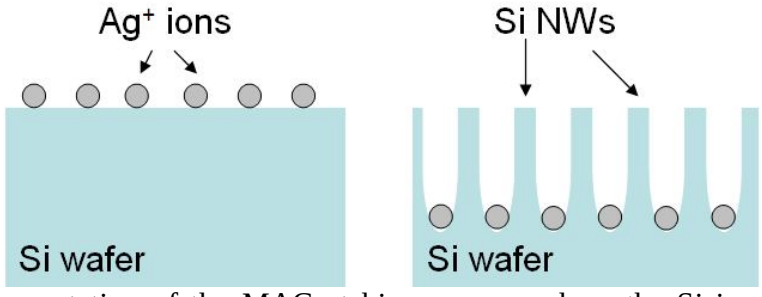

Figure 1. Representation of the MAC etching process where the Si is etched by pore formation to relieve the NWs. Preferential electroless etching occurs in the vicinity of Ag.

Upon removal from the etching bath, samples were washed copiously with deionised water and then treated with concentrated nitric acid to remove unwanted Ag^0

deposition. The length of the NWs is controlled by the etching time and etchant concentration leaving a uniform, effective porous Si layer.

Electrical contacting methodologies to develop low resistance ohmic contacts between the non-metallic substrates and the metal current collectors involved (a) *in-situ* aluminium sputtering on Ar^+ plasma etched substrates (annealed and as-deposited), and (b) the formation of a Cu-In-Ga-Si sandwich after prior removal of the back SiO_2 layer. Current-voltage analysis was performed using a probe station.

SEM of cleaved (011) cross-sections, (001) plan view and individual NWs were examined on a Hitachi S4800 FESEM operating at 5 kV and EDX analysis was performed using a Hitachi SU70 equipped with an Oxford Instruments Oxford Instruments X-max 50 mm^2 solid-state EDX detector. TEM and CBED were conducted on a JEOL 2100F FEGTEM. The NWs were scrapped onto holey carbon copper grids for analysis. For metallization contacting to back sides of wafers, focused ion beam milling and TEM lamella preparation was conducted on a FEI 200 FIBSIMS workstation. A Pt capping layer was used for sample protection during lamella thinning to electron transparency. XPS was performed on a Kratos Axis 165 spectrometer. XRD was conducted on a Philips X'pert MRDPro diffractometer using Cu Kα radiation.

Results and Discussion

Structural characterization of the Si NWs

Figure 2 shows the resulting SiNW layers that are formed using the metal-assisted chemical (MAC) etching approach. Vertical arrays of NWs are formed across the entire surface of the wafer, as shown in the cross-sectional SEM image in Fig. 2(a-c).

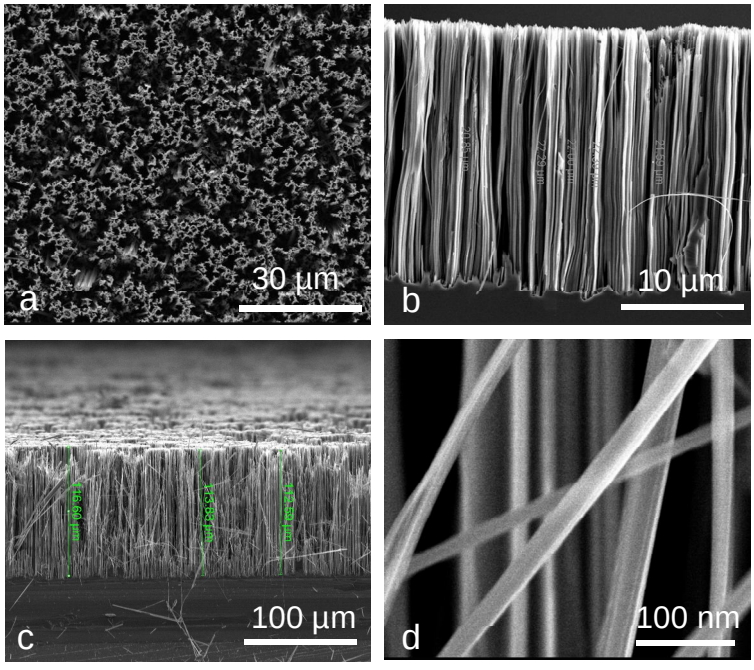

Figure 2. SEM images of the MAC etched Si NWs. (a) Plan views of the NWs showing characteristic clumping. (b,c) Cross-sectional images of the NW-substrate interface and (d) high magnification image several NWs.

High resolution SEM examination reveals that the NWs have lengths dictated by the etching duration: in Fig. 2(b) the NWs are ~20 μm in length and NWs of 115 μm can also be formed, as shown in Fig. 2(c). All NW layers are observed to remain connected to the bulk substrate. Examination of the top surface of the SiNW layers shows that the wires appear in non-uniform distributions characterized by clumped regions of high density NWs and correspondingly, regions of locally less density (Fig. 2a,c). Further examination shows that the less dense regions are not devoid of NWs, rather the NWs are bent towards each other forming the high density regions. This stems from a combination of high length-to-width aspect ratio and capillary forces (12) of high density regions of etched NWs, stemming from drying after liquid immersion from the post-etch cleaning procedure. NWs were measured from SEM images such as Fig. 2(d), to have an average width of 80 nm, for lengths of 115 μm.

TEM analysis summarized in Fig. 3 shows that the NWs have a characteristic rough morphology but maintain a solid core, *i.e.* the non-planar outer surface is unevenly etched and no porosity forms within the NWs. The bright and dark field TEM images in Fig. 3(a,b) and electron diffraction measurements in Fig. 3(c) also confirm their (100) orientation, consistent with etching from bulk Si(100). This non-uniformity in the surface has been shown to be influenced by the doping density (14) and mesoporosity throughout each wire is prevented by judicious choice of the Si resistivity. HRTEM analysis in Fig. 3(c,d) show the roughness of the surface, the presence of a 2-3 nm thick oxide and from the HRTEM image taken down the (111) zone axis of the NW, it is found that the entire wire remains as a diamond cubic structure.

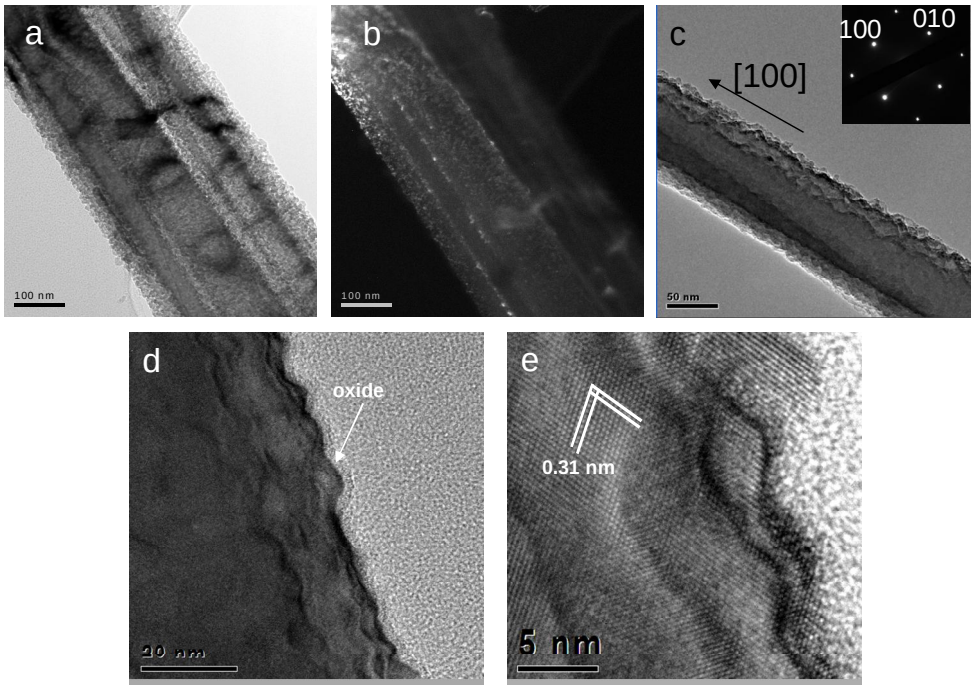

Figure 3. TEM images of the MAC etched Si NWs showing the characteristic roughened outer surfaces. (a) Bright field and (b) high angle annular dark field TEM images of a single rough NW. The main core of the NW is not mesoporous. (c) A larger diameter NW showing roughened surfaces. The inset electron diffraction pattern confirms a diamond cubic structure with a (100) orientation. (d,e) HRTEM image of the NW outer surface showing characteristic roughness, oxide coating and the 0.31 nm {111} interplanar spacing characteristic of diamond cubic Si.

During the electroless etching of these wafers, the electrochemical potential for electron injection/hole consumption depends on the relative position of the Ag^+/Ag^0 redox potential to that of the valence band of the semiconductor. Since the redox potential of Ag^+/Ag^0 lies below the valence band of Si,(15) lower p-type dopant concentrations (*i.e.*, higher Fermi level energy) will cause the bands to bend less and decrease the depletion width at the NW surface (16); etching can proceed efficiently in the presence of the Ag^+ and continued etching at pore walls (NW surfaces) is possible due to non-uniform silver ion distribution on the surface and within pores, so long as the region in question is soaked in the electrolyte. In such case, roughening of pore walls can occur.

To examine the phase purity of the etched NW layers, X-ray diffraction was carried out on both the pristine Si wafer coupons and the resulting Si NW layers. Figure 4 confirms that the overall crystal a structure remains unchanged. The reduced intensity of the NW sample compared to the pristine sample stems from the partially reduced thickness of a complete Si single crystal, *i.e.* the volume fraction of dense Si is reduced. However, no peak broadening characteristics of nanoscale (<10 nm) Si is found from the main Si peaks, confirming that in 80-150 nm diameter wires, there are no Si crystallites nor other phases formed as a result of the etching process.

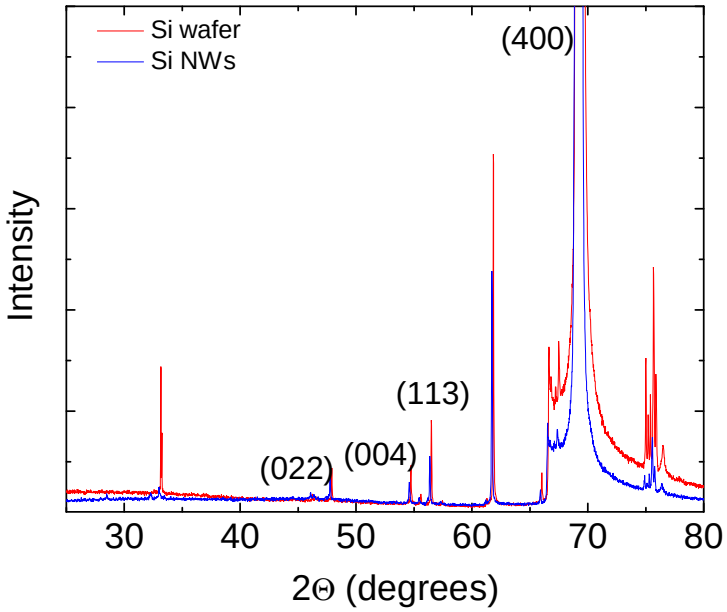

Figure 4. XRD patterns from a Si wafer and a corresponding Si NW sample.

The NWs were investigated by scanning and atomic resolution TEM. Simultaneously, convergent beam electron diffraction patterns were acquired and high order Laue zone (HOLZ) lines from the crystal lattice were monitored as a function of distance across the surface of a single, rough NW. In Fig. 5(a,b), the STEM images confirm that the nanoscale features on the rough NWs stem from non-uniform Si etching at the pore walls during electroless dissolution. No mesoporosity is found through the NWs. In order to assess the influence of roughness on the overall crystal phase of the NWs, 47 CBED patterns were acquired across the NW surface shown in Fig. 5(a). Each pattern was taken at a spatial position separated by 4.2 nm (spot diameter = 1 nm) across 197.4 nm of the NW surface. Snap-shots from the analysis in Fig. 5(c-e) show that the phase and strain sensitive HOLZ lines remained invariant across a surface that is nominally described as

bevelled and rough. In other words, the surface morphology simply stems from the etching processes and the remaining crystal remains as a (100) oriented diamond cubic phase identical to the bulk substrates, with no induced strain, crystallite formation or phase changes resulting from etching.

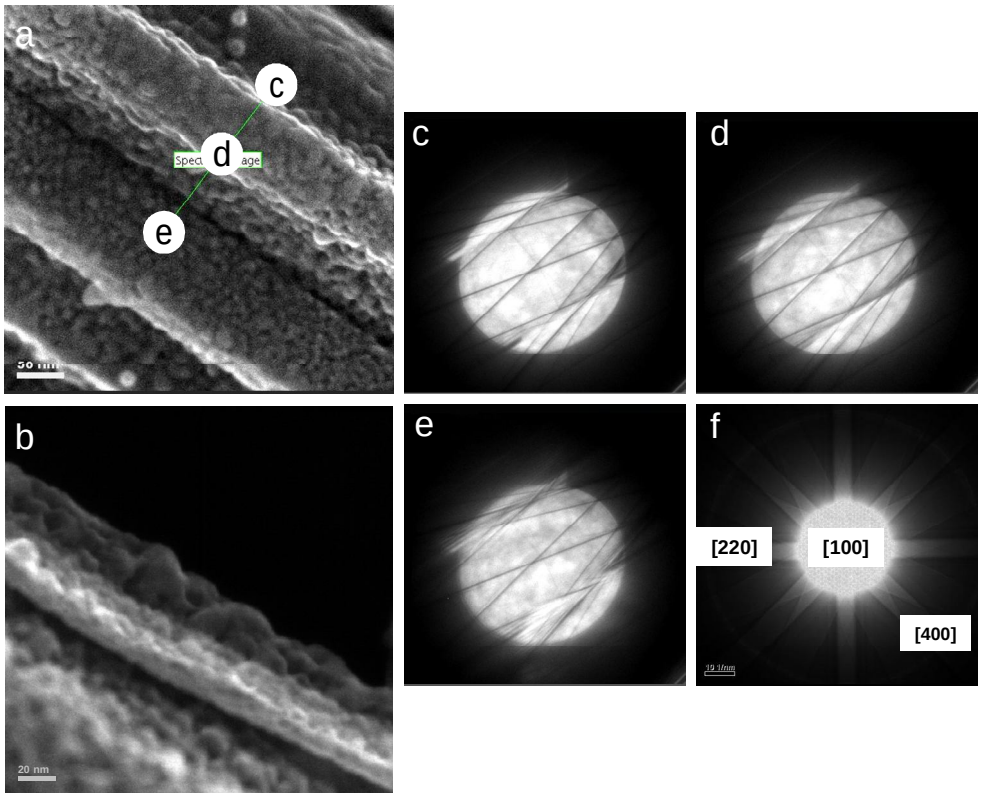

Figure 5. (a) STEM image of a non-uniform NW rough surface. (b) HR-STEM image of the NW surface at a magnification of 1,200,000 × showing the nanoscale roughness features at the outer surface. (c-e) CBED patterns showing characteristics HOLZ lines taken from regions highlighted in (a). (f) Kikuchi pattern along the [100] zone axis of the overall NW confirming its (100) long axis orientation.

Elemental and Compositional Characterization of the Si NWs

The etching process is generally known to leave metallic silver deposits, which are typically removed through a nitric acid-based wash. Owing to strong capillary forces which clump the NWs, the same effect is likely to prevent completely efficient removal of etch-initiators such as Ag and also any reaction products from the electroless dissolution process that are not soluble in solution. Energy dispersive X-ray analysis and X-ray photoelectron spectroscopy of exfoliated Si NWs and Si NW layers were carried out to determine the type of oxide formation on the NW surfaces and to quantify the local and global average concentrations of remnant impurities.

Figure 6(a-c) shows elemental mapping of the Si and O Kα lines from several Si NWs. The Si NWs are predominantly coated with an oxide and it is uniformly distributed (in so far as can be determined taking variable roughness effects into account) along the entire length of the Si NW, consistent with HRTEM analysis in Fig. 3.

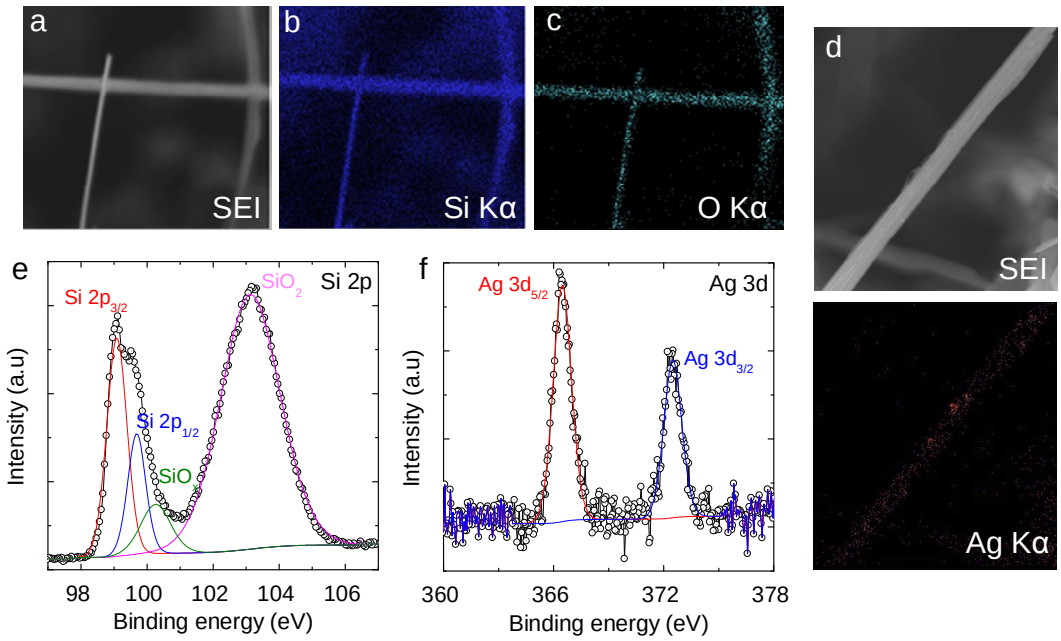

Figure 6. (a-c) EDX mapping of the Si and O Kα X-ray lines showing oxide presence on the surface of NWs. (d) secondary electron image and EDX map of the Ag Kα line on a large NW (e,f) XPS spectra from Si 2p and Ag 3d core-levels.

In Fig. 6(e) the spectra from the Si 2p core-levels are shown. Apart from the hyperfine Si 2p splitting, the presence of SiO_x and SiO_2 is confirmed. Specifically, the NW are predominantly coated with a stoichiometric SiO_2, identical to the bulk substrate, in spite of the roughened surface, which exposes more than just the four {010} planes of nominally square-profile diamond cubic NWs. For larger area investigations (greater density of NWs), the XPS spectra in Fig. 6f indicate the presence of very small quantities of remnant metallic silver from the etching process. This was also seen through EDX mapping, as shown in Fig. 6d. Clear signals from Ag^0 are only found in some areas with a larger density of wider diameter (greater surface area) NWs indicating that the quantity and distribution are sufficiently small. Quantitative measurements of the Ag content shows that the total concentration does not exceed 0.2%. As compared to Au-seeded VLS NW battery anodes that must take into account the irreversible intercalation of Li^+ into the Au, the minute presence of the metallic Ag phase should have minimal effect on specific charge capacity determination.

Obtaining a Suitable Electrical Contact to the Si NW Anode

Because the NWs are inherently part of the original substrate from which they were etched, electrically contacting such anodes with a low resistance, ohmic contact, depends strongly on the conduction type and workfunction of the contact metal. For instance, for lightly doped p-type NW electrodes reported here, the metal workfunction should be close to the semiconducting valence band in order to minimize the Schottky energy barrier between the biased substrate and that of the metal workfunction. A competition exists between the degree of band bending (energy barrier) and the width of the depletion region at the NW surfaces. Classically, Al contacts to Si provide sufficient ohmicity (15). We investigated contacting options involving sputtered Al on the back of the Si NW electrodes *in-situ* following Ar^+ plasma oxide removal. The contact were tested in

sandwich geometries on bulk, unetched substrates to confidently test double-junction ohmicity shown schematically in Fig. 7(a,b). In addition, an In-Ga eutectic was also employed as so that electrical contact could be made to a copper current collector.

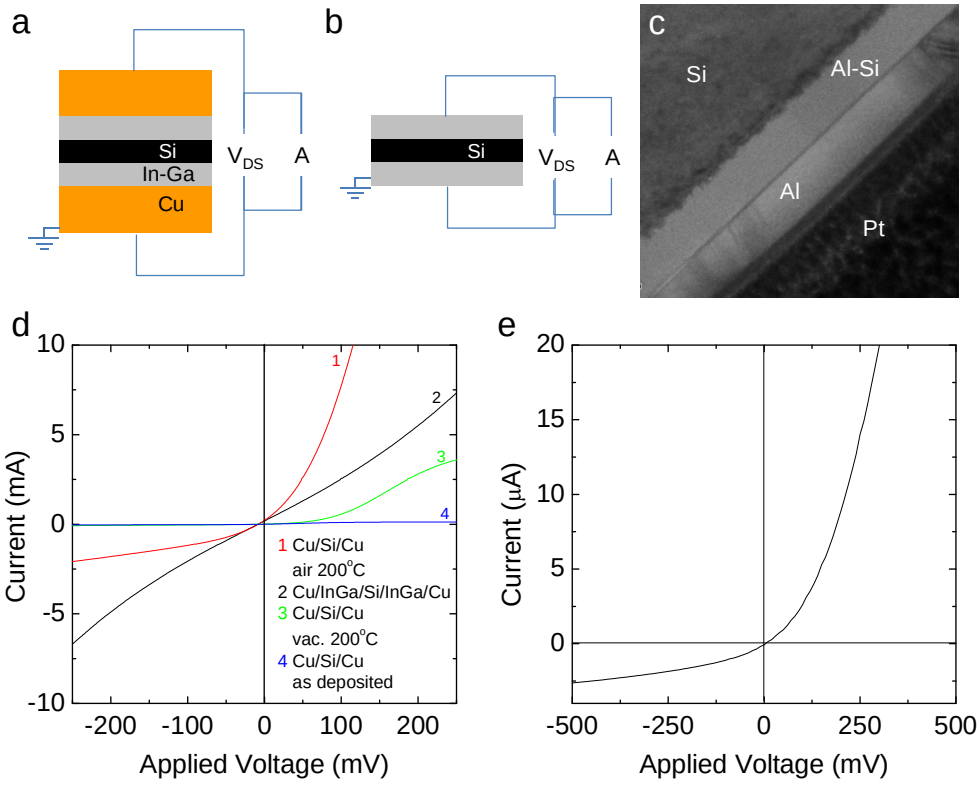

Figure 7. (a,b) Schematic representation of contacting methodologies of Si-based anodes. (c) Bright field TEM image of the oxide stripped, Al-contacted Si backside (unpolished) showing the Al-Si alloy layer. The Pt was used for protection of the lamellar sample during focused ion beam milling. (d) I-V curves from Cu-contacted Si electrodes. (d) I-V curve from Al-contacted oxide-free Si.

Figure 7d shows the characteristic I-V curves from 4 types of contacts: Cu/Si/Cu, Cu/Si/Cu annealed in air, Cu/Si/Cu annealed in vacuum, and a Cu/InGa/Si/InGa/Cu sandwich contact. Due to the smaller workfunction of the copper, the as-deposited I-V exhibited a Schottky-like behavior with very low currents in the μA range. Annealing this contact in air improved contact resistivity thus increasing current flow but retaining the unwanted rectifying response. The In-Ga eutectic on the other hand gives a good ohmic contact between the copper current collector and the Si anode, and is experimentally the quickest and simplest to form and replicate. The ohmic contact gives a single-side contact resistance of ~33-36 Ω talking into account the ohmic drop across the 0.68 mm thick Si wafer with a resistivity of 5-80 Ω cm.

It can be seen from Fig. 7e that direct Al-Si contacting of low-doped Si results in the formation of a Schottky barrier with a low forward bias conductance, preventing ohmicity in the contact. High angle annular dark field scanning TEM and corresponding line-profile EDX analysis of this junction, shown in Fig. 8, confirms the formation of a 25 nm thick Al-Si alloy, as determined from the mixed Al and Si signals in Fig. 8a. The EDX line profiles show a smooth linear gradient in the Al and Si signals indicating a metallurgical junction and not an Al_xSi_y phase. In addition, the thickness of this layer

compared to the Al layer (20 nm) and the constant single values form the O Kα line rule out the formation of amorphous Al_2O_3. The findings are also consistent with localized weak p-n junction formation from within the Si, negating the use of Al for ohmically contacting p-type Si NW electrodes.

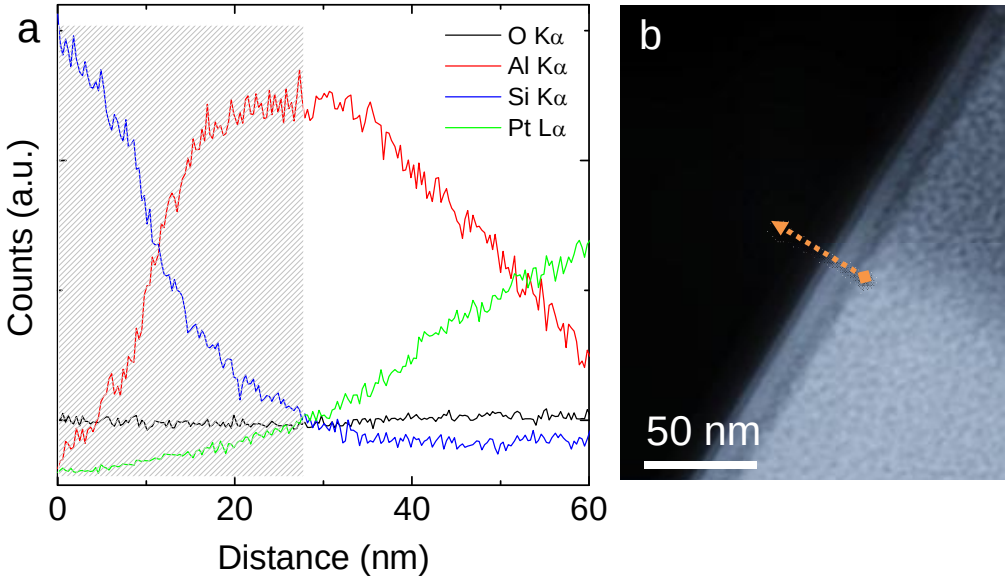

Figure 8. (a) Elemental line scans of X-ray emission from the Si-Al interface. (b) Cross sectional HAADF STEM image of the Si-Al interface between the Al and Si.

Thus, for lightly doped, p-type Si etched to form an array of Si NWs is best contacted using an In-Ga eutectic as an ohmic contact between the Si and copper current collector. Other contacting approaches including Al are still possible with n-type substrates. Having a low resistance contact (17,18) to a NW sample that is fully connected to a bulk crystal wafer is paramount for minimizing both the intercalation potential of Li^+ (*vs.* Li^+/Li), a more uniform SEI formation, and reduction in the overall internal battery resistance. The ease in formation of wafer scale array of NWs allows their potential investigation as high performance lithium-ion battery anodes, without necessitating direct NW growth on current collectors, which typical results in quasi-vertical arrays and random meshes of NWs. By using electroless and also electrochemical etching of Si wafers, nanoscale Si with the structural composition and doping densities identical to the substrate can be used, with an added benefit of inherent NW connectivity to the current collector.

Conclusions

Si NWs have been fabricated by metal assisted chemical etching, where the NW length is controlled through etch process parameters. The NWs have a characteristic rough surface morphology and remain as single crystal and high resolution microscopy techniques conclusively show that the NWs contain no detectable defects compared to the bulk substrate aside from surface roughness and remnant metallic silver from the etch process with a very low (0.2%) concentration. In addition, the NWs are coated with a stoichiometric SiO_2. For application as lithium-ion battery anodes, electrical contacting investigations showed that low resistance, ohmic contacts to Cu current collectors can be achieved using and In-Ga eutectic, whereas Al contacts caused Al-Si mixed phases that

caused p-n junction formation within the Si and significantly lowered conductivity. This approach is a viable method for wafer scale processing of Si NW mats for lithium-ion battery anodes.

Acknowledgments

The authors acknowledge V. Mogili for assistance with STEM imaging. Part of this work was conducted under the framework of the INSPIRE programme, funded by the Irish Government's Programme for Research in Third Level Institutions, Cycle 4, National Development Plan 2007-2013 and also by the 7th Framework Programme, SiNAPS project, Grant Agreement No. 257856.

References

1. B. A. Boukamp, G. C. Lesh, R. A. Huggins, *J. Electrochem. Soc.*, **128**, 725 (1981)
2. U. Kasavajjula, C. Wang, A. J. Appleby, *J. Power Sources*, **163**, 1003 (2007)
3. S. Ohara, J. Suzuki, K. Sekine, T. Takamura, *J. Power Sources*, **136**, 303 (2004)
4. C. K. Chan, H. Peng, G. Liu, K. McIlwrath, X. F. Zhang, R. A. Huggins, Y. Cui, *Nat. Nanotechnol.*, 3, 31 (2008).
5. K. Q. Peng, Y. J. Yan, S. P. Gao, J. Zhu, *Adv. Mater.*, **14** , 1164 (2002).
6. R. Ruffo, S. S. Hong, C. K. Chan, R. A. Huggins, Y. Cui, *J. Phys. Chem. C*, **113**, 11390 (2009).
7. R. Huang, X. Fan, W. Shen, J. Zhu, *Appl. Phys. Lett.*, **95**, 133119 (2009).
8. K. Kang, H. S. Lee, D. W. Han, G. S. Kim, D. Lee, G. Lee, Y. M. Kang, M. H. Jo, *Appl. Phys. Lett.*, **96**, 053110 (2010).
9. Y. Yang, M. T. McDowell, A. Jackson, J. J. Cha, S. S. Hong, Y. Cui, *Nano Lett.*, **10**, 1486 (2010).
10. H. Föll, J. Carstensen, E. Ossei-Wusu, A. Cojocaru, E. Quiroga-Gonzalez, G. Neumann, *J. Electrochem. Soc.*, **158**, A580 (2011)
11. H. Föll, H. Hartz, E. K. Ossei-Wusu, J. Carstensen, O. Riemenschneider, *Phys. Status Solidi (RRL)*, **4**, 4 (2010).
12. K. Q. Peng, Y. Wu, H. Fang, X. Y. Zhong, Y. Xu, J. Zhu, *Angew. Chem. Int. Ed.*, **44**, 2737 (2005).
13. Z. Li, B. Rajendran, T. I. Kamins, X. Li, Y. Chen, R. S. Williams, *Appl. Phys. A*, **80**, 1257 (2005).
14. A. I. Hochbaum, D. Gargas, Y. J. Hwang, P. Yang, *Nano Lett.*, **9**, 3550 (2009).
15. K. Q. Peng, J. J. Hu, Y. J. Yan, Y. Wu, H. Fang, Y. Xu, S. T. Lee, J. Zhu, *Adv. Funct. Mater.*, **16**, 387 (2006).
16. M. I. J. Beale, J. D. Benjamin, M. J. Uren, N. G. Chew, A. G. Cullis, *J. Cryst. Growth*, **73**, 622 (1985).
17. L. F. Cui, L. Hu, J. W. Choi, Y. Cui, *ACS Nano*, **4**, 3671 (2010).
18. C K. Chan, R. N. Patel, M. J. O'Connell, B. A. Korgel, Y. Cui, *ACS Nano*, **4**, 1443 (2010).